JOURNAL OF VIROLOGY, Mar. 2010, p. 2432–2443 Vol. 84, No. 5
0022-538X/10/$12.00 doi:10.1128/JVI.01998-09

Vaccinia Virus Particles Mix Inefficiently, and in a Way That Would Restrict Viral Recombination, in Coinfected Cells[▽]

Y.-C. James Lin and D. H. Evans*

Alberta Institute for Viral Immunology and Department of Medical Microbiology and Immunology, Faculty of Medicine and Dentistry, The University of Alberta, Edmonton, Alberta T6G 2H7, Canada

Received 22 September 2009/Accepted 15 December 2009

It is well established that poxviruses are subjected to genetic recombination, but attempts to map vaccinia virus genes using classical genetic crosses were historically confounded by high levels of experimental noise and a poor correlation between physical and genetic map distances. These virus-by-virus crosses also never produced the 50% recombinant progeny that should be seen in experiments involving distant markers. Poxviruses replicate in membrane-wrapped cytoplasmic structures called virosomes (or factories) and we have developed a method for tracking the development of these structures using live cell imaging and cells expressing phage lambda Cro protein fused to enhanced green fluorescent protein (EGFP). The EGFP-cro protein binds nonspecifically to DNA and permits live cell imaging of developing vaccinia virus factories. Using this method, we see virosomes first appearing about 4 to 5 h postinfection. The early virosomes exhibit a compact appearance and then, after a period of exponential growth lasting several hours, blur and start to dissipate in a process presumably linked to viral packaging. During the growth period, the virosomes migrate toward the nuclear periphery while colliding and fusing at a rate dependent upon the numbers of infecting particles. However, even at high multiplicities of infection (10 PFU/cell), we estimate ~20% of the virosomes never fuse. We have also used fluorescence *in situ* hybridization (FISH) methods to study virosomes formed by the fusion of viruses carrying different gene markers. FISH showed that DNA mixes rather poorly within fused virosomes and the amount of mixing is inversely dependent on the time between virosome appearance and fusion. Our studies suggest that the intracellular movement and mixing of virosomes create constraints that reduce opportunities for forming recombinants and that these phenomena create outcomes reflected in classical poxvirus genetics.

Genetic recombination catalyzes the acquisition of new traits and plays a key role driving virus adaption to new hosts and ecological niches. It can also promote the reassortment of antigenic determinants and facilitate DNA repair and thus aids virus survival in response to evolving immune surveillance and other environmental hazards. Poxviruses provide several classic illustrations of the impact of recombination on viral evolution. For example, the attenuated South American form of variola virus (alastrim or variola minor) is probably a hybrid virus derived from recombination between the more virulent West African and Asian variola strains (10). Malignant rabbit virus is another example of a recombinant virus found in a facility propagating myxoma and Shope fibroma viruses (2). Genome analysis suggests that poxviruses can also slowly accrete homologs of host genes over long periods of evolutionary time. This process selects for acquisition of virulence factors, and each of the poxvirus genera carries a characteristic complement of such genes (23).

Fenner provided the first experimental demonstration of vaccinia virus (VAC) recombination in culture (12), and soon thereafter Dumbell and Bedson produced recombinants between different orthopoxviruses such as variola and rabbitpox viruses (1). Using a variety of methods, we and others have shown that poxvirus recombination uses a simple form of single-strand annealing reaction intimately linked to virus replication (4, 13, 15, 34). An interesting feature of these reactions is that poxviruses can catalyze very high frequency recombination between genetic markers on cotransfected DNAs. Such "four-factor crosses" have shown that among DNAs selected for having undergone at least one intermolecular recombination event between distantly spaced flanking markers, linkage is lost between internal markers when the spacing starts to exceed ~600 nucleotides (24).

The high frequencies of recombination that can be measured using DNAs transfected into poxvirus-infected cells are not consistent with the observation that classical virus-by-virus crosses rarely generate the hypothetical limit of 50% recombinant viruses. This is best illustrated by experiments conducted in the Ensinger and Condit laboratories (7–9, 11, 28). These groups had produced stocks of temperature-sensitive VAC strains and were using marker rescue methods and complementation studies to position the different mutations on the early VAC restriction map. As detailed in the Discussion, these virus-by-virus crosses produced only ~25% recombinant progeny despite using markers spaced up to ~80 kbp apart. In fact, classical virus-by-virus crosses never proved a useful way of mapping poxvirus genes. The best maps were first constructed using marker rescue methods (i.e., testing for reversion of a mutation using transfected restriction fragments) (31) and then later updated using DNA sequencing technologies. It has never been explained what feature of virus biology precludes

* Corresponding author. Mailing address: Department of Medical Microbiology and Immunology, Faculty of Medicine and Dentistry, The University of Alberta, Edmonton, Alberta T6G 2H7, Canada. Phone: (780) 492-2308. Fax: (780) 492-7521. E-mail: devans@ualberta.ca.

▽ Published ahead of print on 23 December 2009.

mapping mutations in this manner or why recombinants are not recovered in the expected numbers.

Classical bacteriophage mating theory provides insights into what factors might limit production of virus recombinants. A key concept is the "mating room," a place where two or more genomes can mix in a way that permits recombination (29). At its simplest, the cell is a mating room and high multiplicities of infection are needed to ensure coinfection with two or more virus genotypes. This is because any virus that replicates in isolation from virus of another genotype will contribute only the parental class of virus to the pool of progeny and will thus reduce the apparent overall recombination frequency. However, at the multiplicities of infection commonly used in virus crosses (~10 PFU per cell), this effect will reduce the 50% limit on recombination by only a few percent. The fact that few poxvirus crosses generate recombinant frequencies in excess of ~25% shows that some other constraint(s) limits cooccupancy of a "mating room." What these constraints might be is not clear.

Poxvirus replication and virion assembly take place in cytoplasmic structures called "factories" or "virosomes" (3, 5). Each virosome likely derives from a single infecting particle and seems to be bounded by a membrane possibly derived from the endoplasmic reticulum (22, 30). Confocal microscopy has been used to detect virosomal substructures, specifically DNA-free channels, and the pattern of proteins expressed from each virosome suggests that most are composed of DNA encompassing a single virus genotype (17). This is consistent with the observation that few mixing events are seen in cells bearing more than one virosome and followed using static (17) or live cell imaging (27). In this communication, we examine in greater detail the extent of interaction between virosomes in coinfected cells and show that the intracellular milieu creates constraints that limit the fusion of coinfecting virus particles and the mixing of different viral DNAs. Virosome fusion would seem to be a logical prerequisite for mixing DNA prior to recombination, and thus these physical constraints on virus-virus interaction can quantitatively explain the long-standing mystery regarding the shortfall in the production of recombinant poxviruses. They also suggest that replicating poxviruses are subject to a previously unrecognized form of "purifying selection" that may help maintain the genetic diversity and integrity of virus populations.

MATERIALS AND METHODS

Viruses, cells, and other reagents. Vaccinia virus (VAC) carrying the T7 RNA polymerase gene inserted in the thymidine kinase locus (vTF 7.5) was obtained from P. Traktman. VAC carrying a β-galactosidase gene inserted in the thymidine kinase (TK) locus was constructed using standard transfection and selection methods and using a *lacZ* gene excised from plasmid pSC66 (VAC TK::*lacZ*). All viruses were grown and titers determined on BSC-40 cells in modified Eagle's medium supplemented with nonessential amino acids, L-glutamine, antibiotics, and antimycotics (all from Gibco) plus 10% fetal calf serum (Sigma). Cells were tested and shown free of mycoplasma.

We also produced a reporter cell line constitutively expressing the bacteriophage λ cro repressor fused to enhanced-green fluorescent protein (EGFP). The *cro* gene was amplified from a phage λ DNA template using the PCR and two primers (forward, 5′ AAGCTTGTATGGAACAACGCATAACCCTGAAAG 3′; reverse, 5′ GGATCCTATTATGCTGTTGTTTTTTTGTTACTCGGGA 3′) and cloned into a Topo PCR 2.1 vector (Invitrogen). The DNA was excised using HindIII and BamHI and recloned into pEGFP-C1 (Clontech). This creates a gene encoding the λ cro protein (66 amino acids) fused to the C terminus of EGFP. The plasmid was transfected into BSC-40 cells using Lipofectamine 2000 (Invitrogen), and recombinants were recovered using G418 selection for neomycin resistance. Individual clones were isolated, and one designated Cro-2 C16 was selected for use in this project based upon a uniform pattern of expression of mostly nuclear green fluorescence. BSC-40 cells were also separately transfected with pEGFP-C1 to produce cloned control cell lines expressing unmodified EGFP.

FISH. The PCR and two sets of primer pairs were to amplify the T7 RNA polymerase (5′ ATGAACACGATTAACATCGCTAA 3′ and 5′ TTACGCGA ACGCGAAGTCC 3′) and *lacZ* (5′ CTCGAGGAATGGGAGATCCCGTCGT TTTAC 3′ and 5′ AAGCTTGCGGCCGCTCAGCTGAATTCCGCCGATAC TGAC 3′) genes using vTF 7.5 and pSC66 templates, respectively, and the PCR products were then cloned into Topo PCR 2.1 vectors. ARES kits (Alexa Fluor 488 for LacZ plasmids and Alexa Fluor 594 for T7 RNA polymerase plasmids) from Molecular Probes and nick translation were used to prepare DNA probes for fluorescence *in situ* hybridization (FISH) analyses. The labeled DNAs were purified using Qiaquick columns and quantified using a Nanodrop spectrophotometer.

For FISH, the VAC-infected Cro-2 C16 cells were fixed for 30 min with ice-cold 4% paraformaldehyde in phosphate-buffered saline (PBS) or overnight at 4°C. The samples and probes were denatured simultaneously at 95°C in hybridization buffer for 5 min in a water bath, chilled in an ice-water bath for 30 s, and then hybridized overnight at 42°C. The hybridization buffer contained 50% (vol/vol) deionized formamide, 2× SSC (300 mM NaCl, 30 mM sodium citrate), 50 mM sodium phosphate (pH 7.4), 1 mM EDTA, 400 μg/ml salmon sperm DNA, 1× Denhardt's solution (Invitrogen), 5% (wt/vol) dextran sulfate, 0.05% (wt/vol) sodium dodecyl sulfate, and 1 to 10 μg/ml fluorescent probe. The samples were washed twice with 50% formamide in 2× SSC at 42°C for 30 min each and then twice with 0.2× SSC at 55°C for another 30 min each. The samples were finally washed with PBS and counterstained with 10 ng/ml DAPI (4′,6-diamidino-2-phenylindole; Molecular Probes) in PBS.

Fluorescence microscopy. All of the fluorescence imaging was performed using an Applied Precision DeltaVision microscope equipped with a temperature-regulated environmental chamber. For live cell imaging, the cells were cultured on optically clear glass-bottom dishes (Fluorodish from World Precision Instruments or gridded μ-dishes from Integrated BioDiagnostics) using phenol red-free modified Eagle's medium (Sigma) supplemented as described above, except that 10 mM HEPES (Gibco) replaced the bicarbonate buffer. The cells were infected with virus for 1 h in PBS at 37°C, and then the inoculum was replaced with fresh warmed growth medium. The dishes were sealed and mounted on the microscope stage, and the temperature was maintained at 37°C. At the end of the second hour, image data were collected at 5-min intervals using Resolve3D software and the fluorescein isothiocyanate (FITC) filter set for EGFP. Static imaging of DAPI, Alexa Fluor 488, and Alexa Fluor 594 reporters used the DAPI, FITC, and/or tetramethyl rhodamine isothiocyanate (TRITC) filter sets, respectively. Using a 100× objective, the pixel dimensions were $x = y = 0.13$ μm and $z = 0.20$ to 1.0 μm, depending upon the thickness of the imaged z plane. The thickness of cells varies over the course of infection, and the depth of the z plane was chosen to minimize the risk of particles moving beyond the image plane. All of the images were subsequently processed using the deconvolution algorithm built into softWoRx (v3.7).

Data processing and analysis. Image data were exported as Photoshop files using softWoRx software and then assembled into composite images using Adobe Photoshop CS3 (v10.3). All of the images were subjected to the same background and scaling adjustments and used only a linear gamma factor. GraphPad Prism (v5.0a) was used to perform statistical analyses of the data. The images shown in Fig. 9C and D were created and analyzed using ImageJ (v1.42). To derive the distances shown in Fig. 10, the map position of each mutation was determined from a description in the literature of either the exact map position (as determined by DNA sequencing), the midpoint of the gene location known from complementation analysis, or the midpoint of the restriction fragment known from marker rescue analysis. In the latter two situations, the location error was estimated as half of the distance between the boundaries of the gene or restriction fragment. The distance error in any given cross was approximated as the average of the location error for each of the two markers used in the cross.

To calculate what effect finite input would have on recombinant production, we used the formula derived by Lennox et al. (19). They demonstrate that the correction factor $F(P)$ at any given multiplicity of infection can be calculated from the formula

$$F(P) = e^{-P} \sum_{N=1}^{\infty} \frac{P^N}{N!} \times \frac{N-1}{N}$$

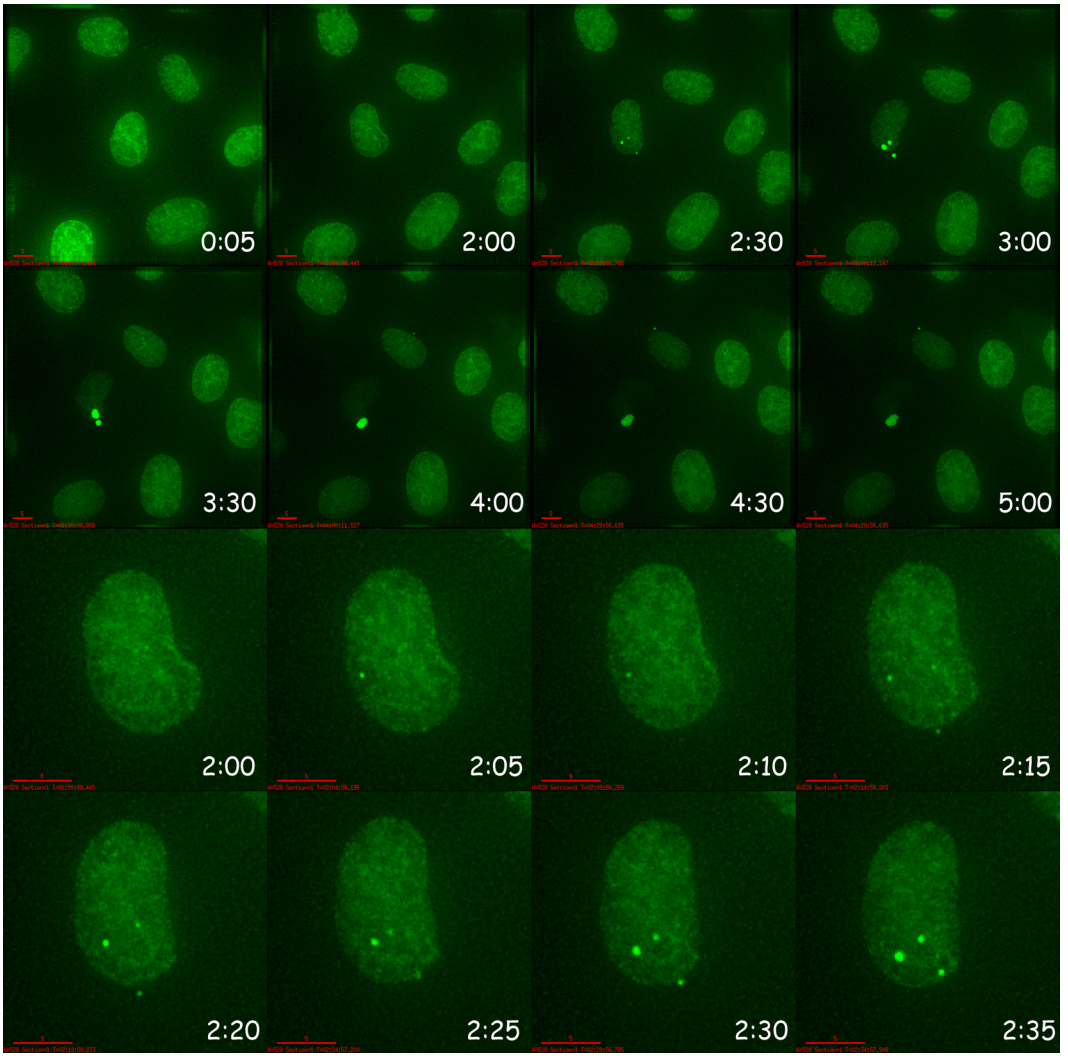

FIG. 1. EGFP tagging of replicating poxviruses. Cro-2 C16 cells, constitutively expressing a DNA-binding EGFP-cro fusion protein, were infected for 1 h with VAC at a multiplicity of infection of 10. After another hour, the dish was transferred to the microscope and an image was recorded every 5 min over the next 5 h. The EGFP-cro protein is initially located in the cell nuclei, but starts to stain three small cytoplasmic structures that appear over a 10-min period about 2 h after the start of imaging (lower six panels). These structures grow over the next 3 h and, in this example, fuse to form a single larger virosome (upper six panels). Note how the initial nuclear fluorescence is selectively lost in infected cells. The red scale bar indicates 5 μm.

where P is the sum of the average multiplicity of infection of each virus and N is the number of particles. We have not incorporated a correction for the number of virus particles that could replicate in a cell (19), as our studies use multiplicities of infection far lower than what has been reported to be achievable in culture (22).

A numerical simulation was used to determine how fusion events would be randomly distributed among coinfecting particles. Ten separate runs of 100,000 iterative simulations were performed and showed that if 5 fusion steps were distributed randomly among 10 interacting virosomes, it would leave an average of 2.20 ± 0.06 virosomes per cell unfused. A detailed description of the algorithm devised by Yin Li, Department of Mathematics and Statistics, University of Alberta, can be supplied upon request.

RESULTS

EGFP tracking of replicating VAC viruses. To follow the fate of replicating viruses, we devised a vital tagging system that uses cells constitutively expressing EGFP fused to the bacteriophage λ cro repressor protein. We had originally hoped to use the EGFP-cro DNA binding protein to selectively tag VAC modified by incorporating the cro repressor binding site. However, adding the six operator binding sites (O_L1 to -3 and O_R1 to -3) to the VAC genome did not significantly alter the amount of EGFP-cro labeling compared to that of an unmodified virus (data not shown). In fact, any of the virosomes formed in these cells can be labeled with the EGFP-cro protein, presumably through a nonspecific DNA binding activity (Fig. 1). This fluorescent label appears to be recruited from a pool of protein located predominantly in the cell nucleus and is sufficiently stable in fluorescence imaging experiments to track the fate of virus particles over time scales up to 10 h. No selective staining of the cell nucleus or of virosomes was detected in cells constitutively expressing just EGFP, showing that the cro peptide is responsible for DNA binding (data not shown). Vaccinia virus also seemed to plate equally well on

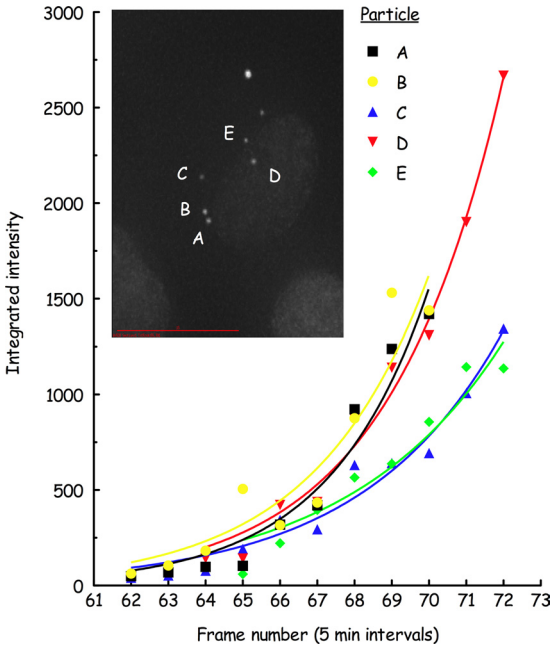

FIG. 2. Tracking virosome growth in VAC-infected cells. Cro-2 C16 cells were infected for 1 h with VAC at a multiplicity of infection of 10. After waiting 1 h, a series of live cell images were then acquired over the next 6 h. In the cell shown here, the first fluorescent particles appeared in frame 62 followed by several others over the next few frames. The integrated intensity of five of the seven fluorescent spots was determined over the next 10 frames (50 min) and corrected to remove any local background fluorescence. The image shown in the inset is frame 70. The nucleus had faded substantially by this point in the infection, although it remains faintly visible in the background of the image. The curves show a best fit to a simple exponential growth equation (R^2 = 0.90 to 0.99) and doubling times that are not statistically different ranging from 9 to 14 min. The red scale bar indicates 15 μm.

EGFP- and EGFP-cro-expressing cells, suggesting that the cro-DNA binding interaction had little or no deleterious effect on virus growth.

This method provides a simple way of tracking the uncoating, movement, and growth of coinfecting VAC particles. Figure 2 shows a cell infected for 1 h at a high (10 PFU/cell) multiplicity of infection and where at least 7 virosomes can be seen. All of these particles "winked" into existence within a relatively short period of time (~20 min) and usually about 4 to 5 h after infecting the cells (i.e., 1 h of infection, 1 h of hold, 2 to 3 h into recording). The timing of virosome appearance varied somewhat from cell to cell, and sometimes viruses weren't seen until as late as ~7 h postinfection. We also noted a reduction in the proportion of infected cells within the imaging fields, compared with cells located in peripheral fields, suggesting that the imaging process may somewhat decrease the efficiency of establishing an infection in some fraction of cells. Because of this variability, the time of virosome appearance served as the most reproducible marker for synchronizing and comparing intracellular events. At first appearance, the size of each spot approximates the limits imposed by the pixel resolution (0.13 μm) and is thus consistent with the dimensions of a VAC particle (~0.2 μm). All of the particles also exhibited a similar initial fluorescence intensity that then increased with time. The initial doubling times ranged from 9 to 14 min for different particles over the first hour of tracking (Fig. 2). The number of particles detected in these experiments generally reflected the multiplicity of infection, suggesting that while the particle/PFU ratio is not known with certainty, these methods probably track the portion of viable plaque-forming virus in these stocks.

Virosome fusion. When one follows the fate of individual virosomes using live cell imaging, we see several examples of virosome fusions. Figure 3 shows a continuation of the image set initially tracked in Fig. 2. In frame 70, one can see two equally bright particles, designated A and B, as well as a third particle that is distinguished from A and B by a slightly reduced fluorescence (C). Five minutes later, this arrangement has been replaced, in frame 71, by just two virosomes and one of these is now substantially brighter than any of the presumed antecedent factories. These two virosomes then continue to grow in size and brightness in the next frame (no. 72). If one integrates the intensity of these particles, it is apparent that the fluorescence of the fusion product (3,785 arbitrary units) represents more than the sum of the fluorescence exhibited by the two presumed parent particles (1,439 + 1,420 = 2,859 units). However, based upon the prior rate of growth of particles A and B (Fig. 2) it can be estimated that each would have increased in intensity by about 40% over a single 5-min frame. If one corrects for this fact, then the larger factory exhibits about 95% of the predicted fluorescence based upon the coalescence and continued growth (at the same rate) of two smaller particles. It should also be noted that a great many virosomes were tracked over the course of this study and if fusion was seen early in the replication cycle, then the resulting particles persisted as stable aggregates.

Genome mixing within virosomes. If one continues to monitor the behavior of these EGFP-tagged virosomes, they typically track toward the nuclear periphery while continuing to grow larger and becoming more asymmetric with time. They also start to lose the compact structure that characterizes early virosomes (Fig. 1). We presume that these visible changes in virosome structure reflect previously characterized transitions from an early DNA replication step in the virus life cycle to a later virus assembly and genome-packaging phase. Collisions between virosomes continued to occur throughout infection, but late in infection, these collisions rarely seemed to disrupt more mature virosomal boundaries. The question then arises regarding whether these fusion events can mix the DNAs of viruses of different genotypes. This is important for the purposes of our study, since the mixing of different coinfecting virus genomes is assumed to be an essential prequel to recombination.

We used fluorescence *in situ* hybridization (FISH) to investigate this question. Cro-2 cells were cultured on gridded dishes, infected with a 1:1 mixture of viruses carrying either the *Escherichia coli lacZ* or T7 RNA polymerase gene, and the distribution of the virus DNA was determined using EGFP fluorescence (Fig. 4, top panel). The dish was removed from the microscope, and the infected cells were fixed and then hybridized to a mixture of two gene-specific FISH probes. The specimens were then counterstained with DAPI and returned to the microscope, and the cells of interest were relocated using the recorded grid position. Although FISH methods

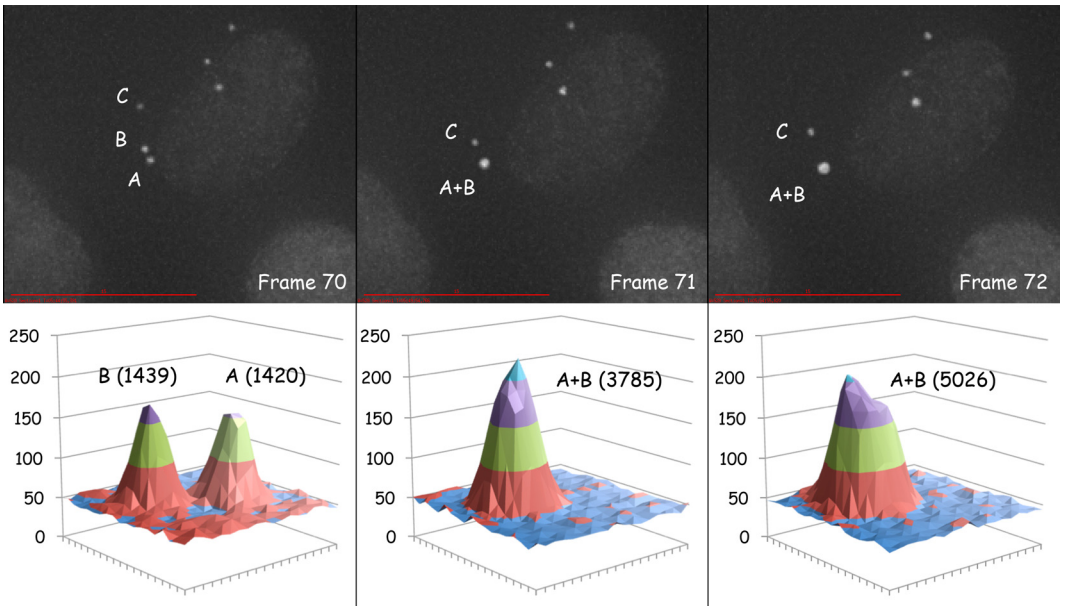

FIG. 3. Virosome fusion. The three upper panels show three consecutive fluorescence images spanning 10 min of virus development. The particles designated A and B seemed to fuse into a single larger and brighter particle (A + B) in the 5 min separating frames 70 and 71. The three lower panels show the distribution of the fluorescence and integrated fluorescence intensities immediately surrounding the fusing virosomes. Note that these images are a continuation of the virosome growth curves shown in Fig. 2. The red scale bar indicates 15 μm.

cause some degradation of the image quality, it is apparent that most of the virosomes, in this example, are composed of DNAs that hybridize to just one of the two FISH probes (Fig. 4, bottom panel). However, one of the virosomes contained a mixture of DNAs, as illustrated by the costaining with both red and green fluorescent probes. Thus, virosome fusion can lead to the DNA mixing that is required for recombination.

Frequency and timing of virosome fusion. Fig. 5 illustrates the method used to determine how often coinfecting virus factories fuse during the process of virus replication. Cells were infected with VAC at multiplicities of infection of 2 or 10, and then a gridded field of 0.5 mm by 0.5 mm was scanned to map where the cells were located. These cells were then tracked over time, and the appearance and fate of any virosomes were followed using EGFP-cro fluorescence over the next ~6 h. Each cell was scored for the number of factories appearing over time, along with the timing and number of fusion events. For example, in this image (Fig. 5) at least 10 virosomes can be detected at the 1:45 time point, only 7 are seen 15 min later (2:00 h), and eventually only 4 mature virosomes are detectible within that cell (4:00 h). At the end of the experiment, each marked cell was recentered in the image field and a full set of *z*-stack images was recorded for each of the infected cells showing the final distribution of fused and intact factories. A composite image showing the relative grid position of each of the imaged cells was also collected. After FISH staining, this reference image was then used to relocate the subset of infected cells and was used to confirm that DNA mixing had occurred (see below).

It is important to note that this method is laborious, and it is impossible to accurately quantify all of the fusion events that might occur in cells infected with many viruses. A particular problem is that VAC-infected cells round up and move in an unpredictable manner during infection (27), and if some *z* planes are not captured in all of the scans over all of the time points, then some smaller virosomes could be missed and their disappearance possibly recorded as fusion. Thus, one cannot reliably track all of the fusion events as a function of virosome number. However, one can determine which fraction of infected cells show no evidence of virosome fusion by counting the number of virosomes at the beginning and end of the experiment. These data are still useful as the number of null events represents the $P(0)$ term in the Poisson equation and can be used to determine the average number of fusion events across cells infected with different numbers of viruses. The results of this analysis are shown in Fig. 6.

Figure 6 summarizes how often virosome fusion happens in VAC-infected cells. As might be expected, the proportion of infected cells exhibiting one or more virosome fusions goes up as the number of virosomes per cell increases. Only rarely are fusions seen in cells infected with two virosomes, and less than half of cells exhibit a fusion event with three infecting particles. However, at high multiplicities of infection, one or more fusions are almost always observed. The number approaches unity at multiplicities in excess of ~7. If one assumes that the frequency of seeing a cell enclosing a virosome fusion is a random event determined by a simple Poisson likelihood, one can estimate from the $P(0)$ term the parameter μ, where μ is the average number of fusions per category of cell type (e.g., cells with 2 virosomes per cell). The parameter μ can be calculated from the formula

$$P(0, \mu) = \frac{\mu^0 \times e^{-\mu}}{0!} = e^{-\mu} \text{ and thus } \mu = -\ln[P(0)]$$

Figure 7 shows a plot of μ values versus the number of

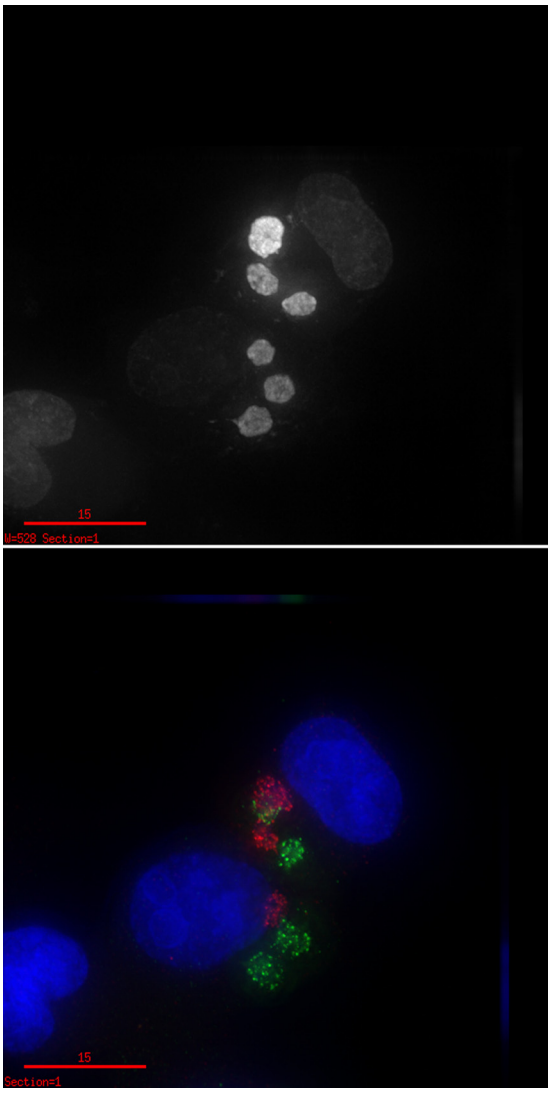

FIG. 4. FISH analysis of virosome composition. Cro-2 C16 cells were coinfected with a 1:1 mixture of VAC carrying the T7 RNA polymerase or *lacZ* gene at a multiplicity of infection of 10 (5 each) for 1 h. After a wait of 1 h, the cells were tracked and this fluorescent image was recorded for 5.5 h after the start of imaging (top panel). The cells were then hybridized to probes specific for the *lacZ* (Alexa Fluor 488) or T7 RNA polymerase (Alexa Fluor 594) gene, stained with DAPI, and reimaged using DAPI, FITC, and TRITC filter sets (bottom panel). Two different infected cells can be seen, each bearing 3 virosomes. The virosome with the brightest EGFP fluorescence virosome, in the upper cell, is composed of sequences hybridizing to two different probes. Note that the EGFP-cro protein is denatured during FISH processing and is thus no longer visible in the second image. The red scale bar indicates 15 μm.

particles per cell. We plotted these values out to only 6 virosomes per cell, because $P(0)$ cannot be measured accurately at higher multiplicities of infection due the rarity of such events. We observed a seemingly linear relationship between the average number of fusions per cell (μ) and the number of virosomes infecting these cells. If we extrapolate these data out to 10 particles/cell (a multiplicity of infection commonly used in recombination studies [see below]), one observes $\mu = 5 \pm 1$ fusion per cell (95% confidence interval [CI]). Collectively, the odds of no fusion occurring in cells infected with 10 viruses become vanishingly small at this multiplicity of infection. Parenthetically, these investigations also provide some insights into the timing of fusion. Although there is much variation from cell to cell, a trend is observed where fusion occurs much faster in cells containing multiple viruses (Fig. 8). For example, if zero is defined as the time of first appearance of the first virosome, it takes on average 65 ± 20 min (mean ± standard error [SE]) for the first fusion event to be detected in cells bearing two virosomes but only about 13 ± 2 min in cells bearing 10 virosomes.

Extent of DNA mixing within fused virosomes. Live cell imaging combined with FISH analysis can also provide insights into the extent of DNA mixing when virosomes do fuse. This is most conveniently illustrated by examining how the two fluorescent hybridization probes are distributed throughout the stack of pixels comprising each three-dimensional image. We used the Cro-2 cells to first track the fate of coinfecting viruses carrying *lacZ* and T7 RNA polymerase genes, located cells that exhibited one or more fusion events, and then used FISH to differentiate between the two infecting VAC genomes. Figure 9A shows an example of one of these FISH images along with a plot showing how the red fluorescence (617 nm) and green fluorescence (528 nm) are correlated within the bicolored image stack seen lying immediately adjacent to the cell nucleus ($R = 0.43$; Fig. 9B). The image shown in Fig. 9A was also used to create a three-dimensional model of how the two signals were distributed within this fused virosome. These are shown in two views looking either down from the top of the image, as also seen in panel A (i.e., along the *z* axis, panels C1 to C3), or in the *x-y* plane looking toward the side of the factory facing away from the cell nucleus (Fig. 9D1 to D3). By separating the image into the two-component green and red FISH signals (Fig. 9C2 and D2 and C3 and D3, respectively) one can see that the virosome contains a complex distribution of the two hybridization targets, which overlap along the boundaries to generate the yellow signal seen in panels C1 and D1.

This analysis was extended to study the variation in the amounts of mixing following a number of different fusion events. We noted that the extent of fusion varied greatly from cell to cell, as judged by a range of correlation factors for the red-green overlap ranging from no overlap ($R = 0$) to $R = 0.65$ (Fig. 9, lower panel). Curiously one never sees a late virosome exhibiting a homogeneous yellow mixture of the two signals, suggesting that although fusion does occur at various points in the development of each factory, this rarely leads to complete mixing of the antecedent particles. Because each of these data points was associated with a live cell video, we could also test whether the time between the appearance of each virosome and its subsequent fusion affected the degree of mixing as determined by the spectral overlap of the two FISH probes (i.e., as shown in Fig. 9B). Although these data are noisy and the correlation is thus limited ($r^2 = 0.25$), the slope of the curve is significantly negative and suggests that the longer it takes for virosomes to fuse, the less opportunity there exists over the course of the virus life cycle to mix the two viral DNAs.

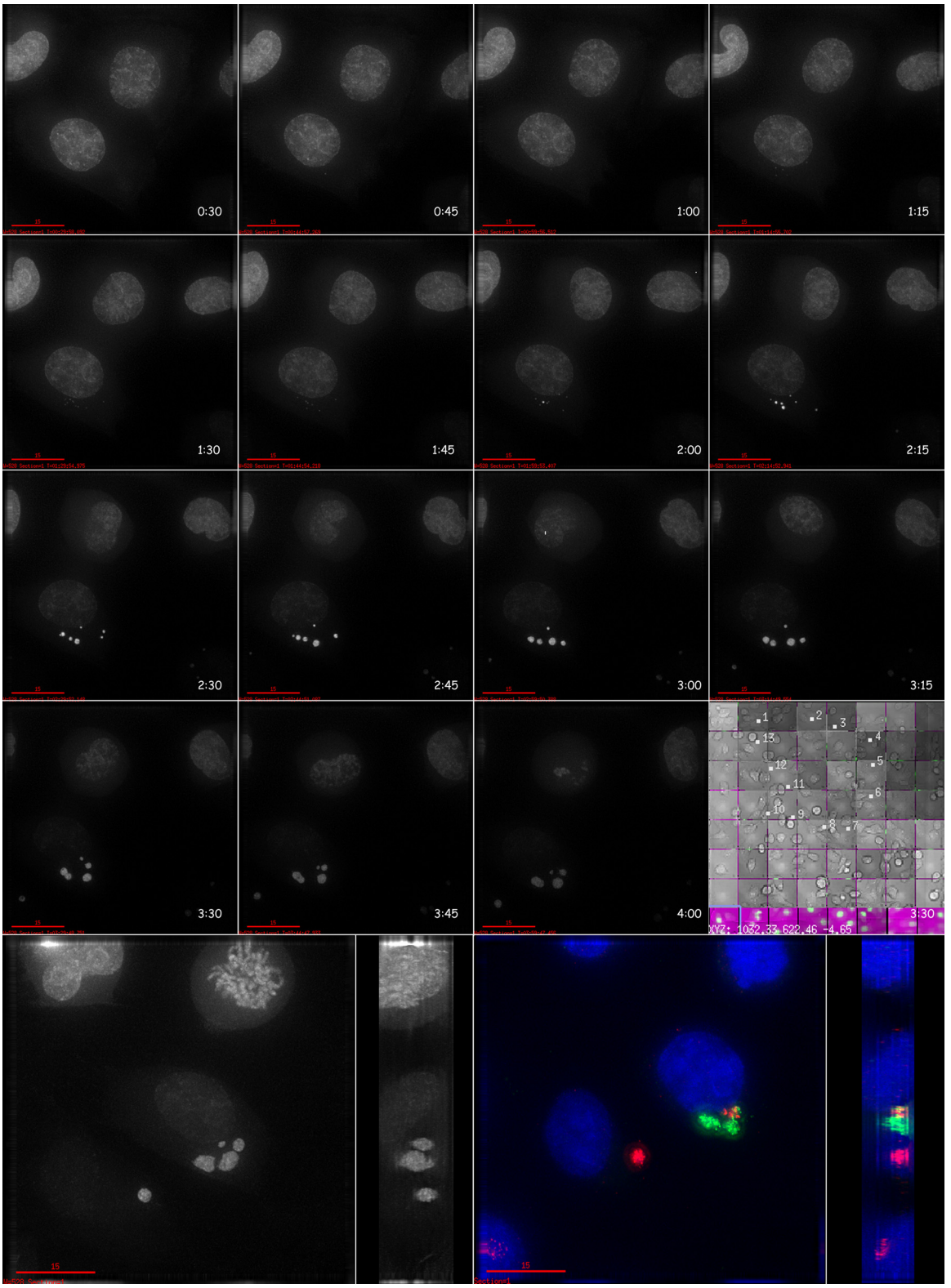

FIG. 5. Live cell tracking of virosome movement. Cro-2 C16 cells were infected for 1 h with a 1:1 mixture of VAC carrying the T7 RNA polymerase or *lacZ* gene, at a multiplicity of infection of 10. After a wait of 1 h, the movement of the virosomes was tracked using EGFP-cro fluorescence over the next 4 h, taking images 5 min apart. The figure shows a subset of the fluorescent images to illustrate the behavior of the factories. These start 30 min into the study and are presented 15 min apart. At the end of the tracking phase, a final image was captured in the *x-y* and *z* planes (bottom left panel) and a low-magnification composite image was prepared to aid in relocating these cells (gray-checkered panel). The cells were then processed for FISH and stained with DAPI and reimaged in the *x-y* and *z* planes using appropriate filters (bottom right panel). Up to 10 particles are visible at the 1:45 time point; these are reduced to just 4 by the end of the experiment, of which one seems to comprise a mix of two different DNAs. The red scale bar indicates 15 μm.

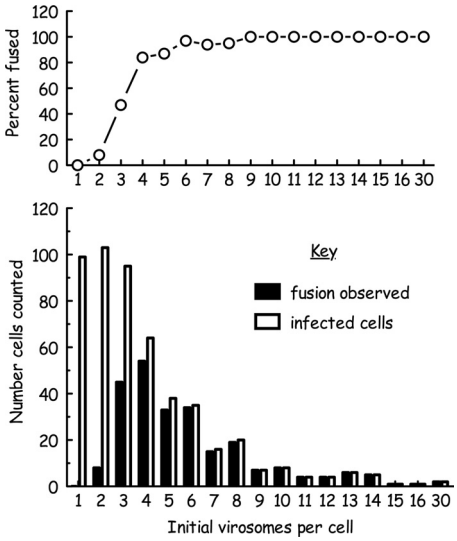

FIG. 6. Fusion events in VAC-infected cells. Cro-2 cells were infected for 1 h with a 1:1 mixture of VAC carrying the T7 RNA polymerase or *lacZ* gene, at a multiplicity of infection of either 2 or 10. After waiting 1 h, the movement of the virosomes was then tracked using EGFP-cro fluorescence over times ranging up to 3 h, taking images 5 min apart. The plot shows what fraction of infected cells imaged (white bars) exhibited at least one fusion event (solid bars) as a function of the initial number of virosomes per cell. The number of virosomes per cell is more difficult to determine at higher viral loads and should be viewed as approximate at high multiplicities of infection (>10 virosomes per cell).

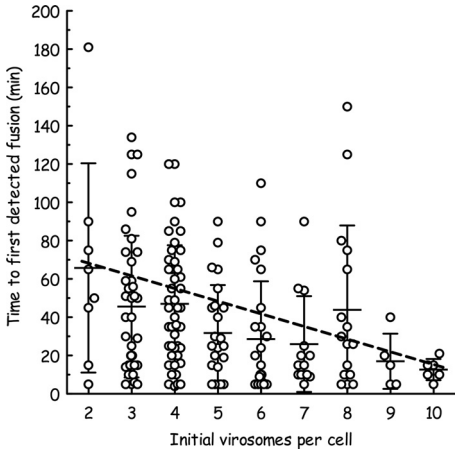

FIG. 8. Timing of virosome fusion. The figure plots the timing from the appearance of the first viral particle to the time when the first fusion was detected. The error bars indicate the mean ± standard deviation. The average time to first fusion (and the standard deviation) decreases with increasing numbers of viruses per cell.

DISCUSSION

We have used live cell imaging methods to track the fate of replicating vaccinia viruses. These studies show that when cells are coinfected with multiple viruses, only a subset of virosomes interact in a manner that produces stable fusions between virus factories. Furthermore, few of the fused particles exhibit an intimate mixture of different DNAs, as judged by FISH methods (Fig. 9). The timing, frequency, and extent of virus fusion are all affected by the multiplicity of infection, but even in cells infected by large numbers of viruses, a portion of the virosomes apparently avoid fusion. The fact that coinfecting viruses interact poorly, or not at all, within the intracellular milieu can explain why too few recombinant viruses are recovered from classical genetic crosses.

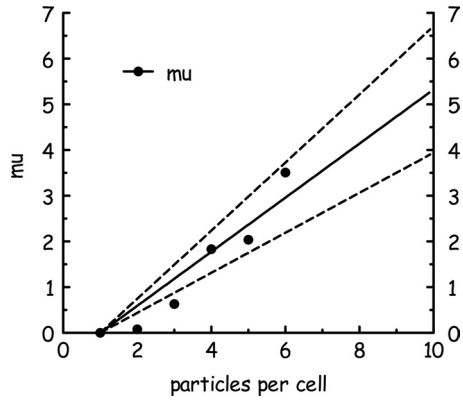

FIG. 7. Estimating virosome fusion frequency as a function of the multiplicity of infection. We used the Poisson formula and the proportion of infected cells showing no evidence any fusions (Fig. 6) to estimate μ, the average number of fusions expected to occur as a function of the number of viruses per cell. The linear regression analysis suggests that an average of about 5 ± 1 virosome fusions would occur in a cell initially infected with 10 viruses. The dashed lines show the 95% confidence intervals. The least-squares fit was constrained to intercept $\mu = 0$ (i.e., zero fusions), where there is only 1 particle per cell. See text for details.

The method makes several simplifying assumptions, not all of which can be tested experimentally. In particular, it is not certain that virosome fusion is essential for recombination or how mixing relates to the efficiency of recombination. However, it would seem reasonable to assume that some mixing of virus DNAs is required prior to or during virus DNA replication. This is when replication-dependent virus recombination has been detected by other methods (13, 33), and the fact these virosomes are replicating while they are also fusing is illustrated by exponential growth we see in the amounts of EGFP-cro binding virus DNA (Fig. 2). We cannot also be certain that our methods capture every fusion event, especially early ones, which could be obscured by the background from nuclear EGFP-cro or because fusion happens at a time preceding or coincident with the appearance of uncoated viruses. However, the fact that viruses typically appear with a similar initial fluorescence (Fig. 2) suggests that there aren't many early fusion events missed by our approach. We are also assuming that each of these early EGFP-cro-labeled particles represents a single virus captured at the point where uncoating makes the viral DNA accessible to EGFP-cro protein. This is consistent with the dimensions of the signal, but our methods couldn't differentiate two particles fused within a space smaller than the limits of the microscope's resolution. Finally, in modeling these events, we are assuming that they are all randomly driven processes unbiased by the history or genetic properties of particular virosomes.

The EGFP-cro fusion protein offers many advantages for live cell imaging of poxviruses. We had hoped that cro's high

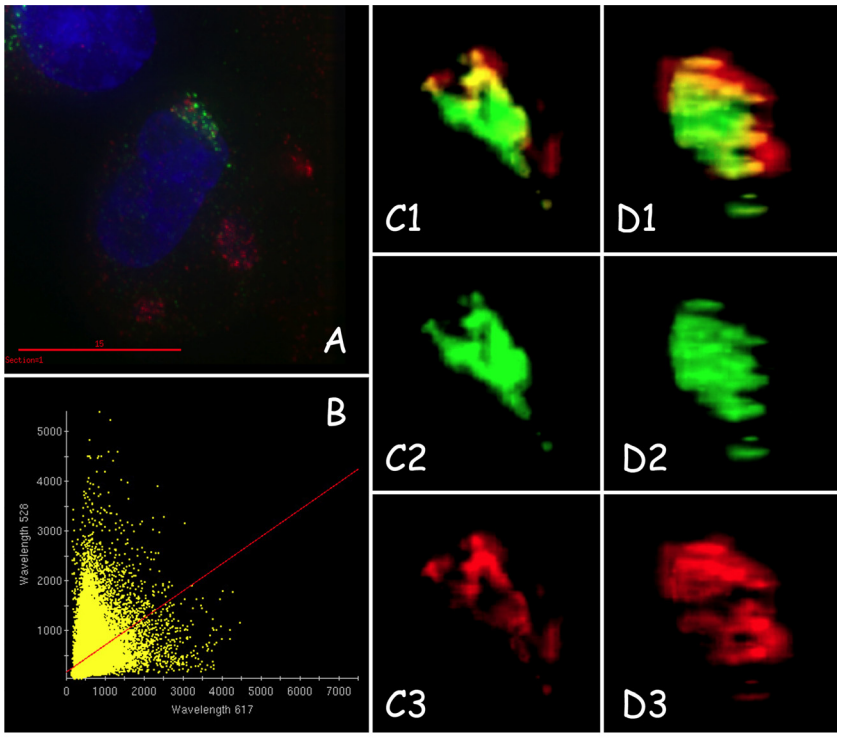

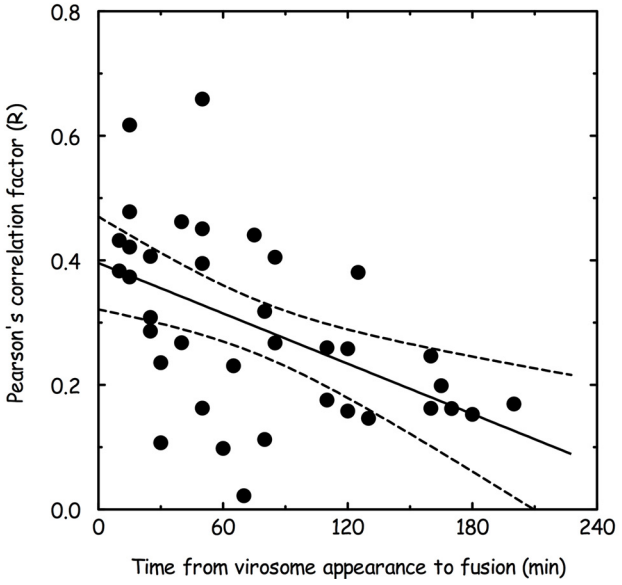

FIG. 9. Degree of virosome mixing as judged by FISH. Cro-2 cells were infected for 1 h with a 1:1 mixture of VAC carrying the T7 RNA polymerase or *lacZ* gene, at a multiplicity of infection of 10, held for 1 h, and tracked for up to 4 h. The cells were then processed for FISH, stained with DAPI, and reimaged. Panel A illustrates the original image, where a virosome formed by the earlier fusion of 2 (or possibly 3) particles is seen lying adjacent to the nucleus and enclosing DNAs containing both *lacZ* (green) and T7 RNA polymerase (red) genes. The relative red and green signal intensities were determined for each of the voxels comprising this image; a plot of these data exhibits a correlation coefficient of 0.43 (B). Panels C1 to -3 and D1 to -3 illustrate a reconstructed model of the virosome viewed either in the same orientation as in panel A (C1 to -3) or in the *x-y* plane, looking toward the virosome and the nucleus (D1 to -3). Panels C1 and D1 show mergers of the separate images seen in panels C2 and C3 and D2 and D3, respectively. The process illustrated in panels A and B was repeated for a number of different virosomes, formed by the fusion of 2 or more particles over 4 h of imaging. The lower panel shows a plot of the correlation between red and green probe distribution and the time taken to observe the first fusion event in this population. A least-squares linear regression and 95% confidence limits are also shown.

affinity for repressor binding sites could be used in combination with a virus encoding multiple binding sites (O_L1 to -3 and O_R1 to -3), to provide a tool for selectively labeling VAC encoding these sites. We produced such a virus, but although the cro-operator dissociation constants (K_ds) are at least as favorable as for the LacI-based systems that have previously been used to tag replicating poxviruses (6, 14, 18), this strategy still cannot provide sufficient selectivity to clearly differentiate

viruses encoding six operator binding sites from wild-type viruses. In hindsight, the ~200-fold difference in Cro's affinity for operator-containing versus nonspecific DNA (6) is probably insufficient to create the specificity we need. However, the reporter still serves as an excellent marker for virus DNA and thus provides a convenient tool for live cell imaging of replicating viruses. Although the EGFP-cro fusion protein has no nuclear transport signal, it is smaller than the nuclear pore limits and much of the protein is found in the nucleus in uninfected cells. It appears to traffic outward and bind to virus DNA over the course of infection. Many other infected-cell proteins are also recruited from the cell nucleus by poxviruses—e.g., barrier to autointegration factor (BAF) protein (32) and topoisomerase II (20)—but whether by an active or passive transport process remains unclear. The gradual loss of fluorescence over time occurs selectively in infected cells and presumably reflects a combination of protein turnover and virus destabilization of host cell mRNAs (25, 26). The rate of increase in virosomal fluorescence will be determined by several factors (e.g., EGFP-cro turnover, rates of recruitment to virosomes, and rates of DNA synthesis) and probably cannot be directly correlated with rates of viral replication. However, the initial estimates of doubling time as deduced from the rate of fluorescence increase (Fig. 2; 9 to 14 min) do approximate the rates that can be measured using Southern blotting for virus DNA (21).

These methods clearly show that some coinfecting virus particles never seem to mix, or mix only poorly, and this can partially explain the aforementioned shortfall in recombinant virus production. Figure 10 shows a meta-analysis of the classical VAC intergenic cross data. These data were culled from the published literature and updated (where possible) to include estimates of the marker positions on the VAC genome. These data represent many different crosses between temperature-sensitive markers and span distances up to about one-third of the VAC genome (8, 9, 11, 16, 28). Two features of these data are immediately obvious. The first is the substantial experimental scatter, and the second is the difficult to define, but clearly not 50%, recombination limit. We suggest that the experimental scatter is actually an intrinsic feature of virus biology and can be explained by variation in the timing of fusion (Fig. 8) combined with variable degrees of mixing within fused virions (Fig. 9). We also suggest that the ~25% recombination limit reflects a combination of effects caused by poor mixing of virus DNAs and by the failure of fusion of some coinfecting virosomes.

One classical explanation for why phage and virus crosses don't produce 50% recombinants arises from the manner in which genomes distribute during infection (19, 29). For example, if a cell were infected by just one of the two parental viruses (virus A or virus B), it could never produce a recombinant. Furthermore, in cells infected by two virus particles, half of the cells will receive two parental viruses (A + A or B + B) and half a mixture of both genotypes (A + B or B + A). In any such infections, replication will contribute only the two parental classes of virus to the pool of progeny and thus reduce the proportion of recombinants. However, if one tests for what effect a finite input of virus would have on R_f, it is apparent that at high multiplicities of infection, the capacity to reduce the yield of recombinants is not large enough to explain the dis-

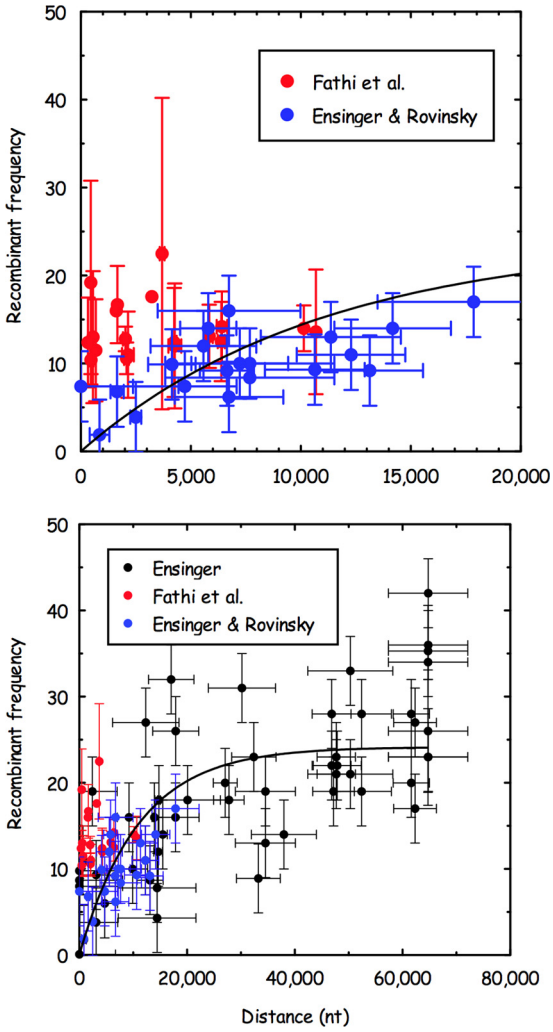

FIG. 10. Meta-analysis of VAC recombination frequencies versus distance data. These data were compiled from reports of intergenic crosses involving VAC-encoded temperature-sensitive mutations (7–9, 11). All of these studies used similar experimental conditions (a 1:1 ratio of each virus at a combined multiplicity of infection of 10) and spanned distances ranging up to ~70 kbp. The physical location of the Condit mutations (red points) is generally known with precision, but most of the Ensinger mutations have been mapped only to a particular restriction fragment. In these cases, the distance error (blue and black horizontal error bars) was estimated from the size(s) of the restriction fragment(s) in which the mutation(s) resides (see Materials and Methods). Fathi et al. reported actual standard deviations for each of the R_f determinations (red-colored points with vertical error bars) (11). The error in R_f is unknown for most of the individual crosses reported by Ensinger (7–9), but as a guide we show an estimated average absolute error of ~4% based upon what was reported for a subset of R_f measurements (7). The solid curve shows a fit to a simple exponential recombination function (29), $R_f = R_f\,(\max) \times (1 - e^{-KD})$, where K is a constant (related to linkage distance) and D is the actual physical distance. The best fit suggests that R_f (max) = 24% with the 95% confidence interval 21 to 27% and $R^2 = 0.25$. Because many of the crosses cluster at distances less than 20 kbp apart (lower panel), we show an expanded view of that region in the upper panel. Note that all of these authors included a 2-fold correction for the loss of a doubly mutant reciprocal class of recombinant virus, and that correction is retained here.

crepancies. For example, most of the crosses shown in Fig. 10 employed a multiplicity of infection of ~10, and under these conditions, the maximum R_f, R_f (max), would be reduced to ~45% (19).

This limit for R_f (max) would be reduced further by the failure of some virosomes to fuse, even at these high multiplicities of infection. We estimated that an average of 5 ± 1 fusion events happen over ~3 h in a cell initially bearing 10 virosomes (Fig. 7 and 8). If we assume these 5 events are randomly distributed among 10 coinfecting particles, a numerical simulation can be used to calculate that on average 22% of the particles will never fuse during a period spanning the onset of replication through what appears (based upon a lack of further growth and the dissolution of the virosome) to be the start of virus packaging. This 22% of the virus will replicate but can produce only parental-type progeny, while the other 78% of viruses could presumably generate up to equal numbers of parental (P) and recombinant (R) progeny if the gene markers are unlinked. If we assume that the yields of progeny virus are equal and proportional regardless of any interaction history, then $R_f = R/(P + R) = 39R/(22P + 39P + 39R) = 39\%$. This effect would reduce the R_f (max) to 39%.

The revised prediction for R_f (max) is still higher than the 21 to 27% seen in classical crosses (Fig. 10), and we suggest that the limited mixing of DNA within the virosomes (Fig. 9) could cause a further reduction in recombinant formation. For example, in this particular case only 44% of the red (VAC vTF 7.5) volumetric pixels (voxels) also exhibit a signal in the green (VAC TK::*lacZ*) channel and 16% of the green voxels also exhibit a red signal. It is difficult to deduce what this measurement actually means in biological terms, because FISH methods may alter the structure of the virosome and thus there is no assurance that the distribution of the fluorescent probes necessarily reflects the original path or distribution of the DNA. However, at multiplicities of infection of 10, the time from viral appearance to fusion is only ~15 min (Fig. 8) and one can crudely estimate from Fig. 9 (bottom panel) that the average amount of mixing would then resemble what is seen in the example image shown in Fig. 9 (top panel). In this image, only ≈30% [30% = (44% + 16%)/2] of the FISH-labeled voxels contain a mix of two genomes. If the example is representative of general trends, and only 30% of the DNAs mix in a way that could produce recombinants at high multiplicities of infection, then R_f (max) would be reduced to ≈15% [$15\% = 15R/(70P + 15P + 15R)$]. Although the magnitude of this effect is uncertain, for the reasons outlined above, the potential for also reducing recombination frequencies is clear.

In conclusion, these studies suggest that the intracellular movement and mixing of virosomes create constraints that reduce opportunities for generating recombinants and that these phenomena create outcomes reflected in classical poxvirus genetics. Perhaps more intriguingly, these observations generate new insights into factors affecting poxvirus evolution. Katsafanas and Moss have used VAC strains encoding core proteins tagged with cyan and yellow fluorescent proteins to show that some virus-encoded gene products aren't randomly distributed throughout infected cells (17). Instead, these particular late gene products are synthesized either close to, or within, the virosome presumed to encode them. Our data suggest that even in cells infected with many virus particles, a significant portion never fuse or fuse only late in the replication cycle and thus likely replicate partly in genetic isolation. These constraints on complementation and recombination would impose a previously unrecognized form of purifying selection on replicating poxviruses, which could help maintain the genetic integrity of virus populations and laboratory stocks. For example, it would prevent the accumulation of defective interfering particles since a "mutant" virosome could have difficulties recruiting complementing factors from other coinfecting particles. Thus, a virosome may be more than just a site of poxvirus replication and assembly. These observations raise the intriguing possibility that virosomes represent an adaption used by poxviruses to compete, in a Darwinian sense, with other poxviruses for intracellular resources.

ACKNOWLEDGMENTS

We thank Nick Li and Michelle Shih for help producing the Cro-2 C16 cell line, Chad Irwin for measuring the plating efficiency of virus on Cro-2 cells, and Chad Irwin and other laboratory members for helpful comments. Yin Li (Department of Mathematics and Statistics, University of Alberta) kindly devised the algorithm used to calculate the proportion of nonfused virions in cells.

This project was funded by awards from the CIHR, NSERC, CFI, and ASRIP (to D.H.E.).

REFERENCES

1. **Bedson, H. S., and K. R. Dumbell.** 1964. Hybrids derived from the viruses of alastrim and rabbit pox. J. Hyg. (London) **62:**141–146.
2. **Block, W., C. Upton, and G. McFadden.** 1985. Tumorigenic poxviruses: genomic organization of malignant rabbit virus, a recombinant between Shope fibroma virus and myxoma virus. Virology **140:**113–124.
3. **Cairns, J.** 1960. The initiation of vaccinia infection. Virology **11:**603–623.
4. **Colinas, R. J., R. C. Condit, and E. Paoletti.** 1990. Extrachromosomal recombination in vaccinia-infected cells requires a functional DNA polymerase participating at a level other than DNA replication. Virus Res. **18:**49–70.
5. **Dales, S., and L. Siminovitch.** 1961. The development of vaccinia virus in Earle's L strain cells as examined by electron microscopy. J. Biophys. Biochem. Cytol. **10:**475–503.
6. **Dong, F., S. Spott, O. Zimmermann, B. Kisters-Woike, B. Muller-Hill, and A. Barker.** 1999. Dimerisation mutants of Lac repressor. I. A monomeric mutant, L251A, that binds Lac operator DNA as a dimer. J. Mol. Biol. **290:**653–666.
7. **Ensinger, M. J.** 1982. Isolation and genetic characterization of temperature-sensitive mutants of vaccinia virus WR. J. Virol. **43:**778–790.
8. **Ensinger, M. J., and M. Rovinsky.** 1983. Marker rescue of temperature-sensitive mutations of vaccinia virus WR: correlation of genetic and physical maps. J. Virol. **48:**419–428.
9. **Ensinger, M. J., J. P. Weir, and B. Moss.** 1985. Fine structure marker rescue of temperature-sensitive mutations of vaccinia virus within a central conserved region of the genome. J. Virol. **56:**1027–1029.
10. **Esposito, J. J., S. A. Sammons, A. M. Frace, J. D. Osborne, M. Olsen-Rasmussen, M. Zhang, D. Govil, I. K. Damon, R. Kline, M. Laker, Y. Li, G. L. Smith, H. Meyer, J. W. Leduc, and R. M. Wohlhueter.** 2006. Genome sequence diversity and clues to the evolution of variola (smallpox) virus. Science **313:**807–812.
11. **Fathi, Z., L. M. Dyster, J. Seto, R. C. Condit, and E. G. Niles.** 1991. Intragenic and intergenic recombination between temperature-sensitive mutants of vaccinia virus. J. Gen. Virol. **72:**2733–2737.
12. **Fenner, F., and B. M. Comben.** 1958. Genetic studies with mammalian poxviruses. I. Demonstration of recombination between two strains of vaccinia virus. Virology **5:**530–548.
13. **Fisher, C., R. J. Parks, M. L. Lauzon, and D. H. Evans.** 1991. Heteroduplex DNA formation is associated with replication and recombination in poxvirus-infected cells. Genetics **129:**7–18.
14. **Fuerst, T. R., M. P. Fernandez, and B. Moss.** 1989. Transfer of the inducible lac repressor/operator system from Escherichia coli to a vaccinia virus expression vector. Proc. Natl. Acad. Sci. U. S. A. **86:**2549–2553.
15. **Gammon, D. B., and D. H. Evans.** 2009. The 3′-to-5′ exonuclease activity of vaccinia virus DNA polymerase is essential and plays a role in promoting virus genetic recombination. J. Virol. **83:**4236–4250.
16. **Kato, S. E., N. Moussatche, S. M. D'Costa, T. W. Bainbridge, C. Prins, A. L. Strahl, A. N. Shatzer, A. J. Brinker, N. E. Kay, and R. C. Condit.** 2008. Marker rescue mapping of the combined Condit/Dales collection of temperature-sensitive vaccinia virus mutants. Virology **375:**213–222.

17. **Katsafanas, G. C., and B. Moss.** 2007. Colocalization of transcription and translation within cytoplasmic poxvirus factories coordinates viral expression and subjugates host functions. Cell Host Microbe **2:**221–228.
18. **Kim, J. G., Y. Takeda, B. W. Matthews, and W. F. Anderson.** 1987. Kinetic studies on Cro repressor-operator DNA interaction. J. Mol. Biol. **196:**149–158.
19. **Lennox, E. S., C. Levinthal, and F. Smith.** 1953. The effect of finite input in reducing recombinant frequency. Genetics **38:**508–511.
20. **Lin, Y. C., J. Li, C. R. Irwin, H. Jenkins, L. DeLange, and D. H. Evans.** 2008. Vaccinia virus DNA ligase recruits cellular topoisomerase II to sites of viral replication and assembly. J. Virol. **82:**5922–5932.
21. **Magee, W. C., K. A. Aldern, K. Y. Hostetler, and D. H. Evans.** 2008. Cidofovir and (S)-9-[3-hydroxy-(2-phosphonomethoxy)propyl]adenine are highly effective inhibitors of vaccinia virus DNA polymerase when incorporated into the template strand. Antimicrob. Agents Chemother. **52:**586–597.
22. **Mallardo, M., E. Leithe, S. Schleich, N. Roos, L. Doglio, and J. Krijnse Locker.** 2002. Relationship between vaccinia virus intracellular cores, early mRNAs, and DNA replication sites. J. Virol. **76:**5167–5183.
23. **McLysaght, A., P. F. Baldi, and B. S. Gaut.** 2003. Extensive gene gain associated with adaptive evolution of poxviruses. Proc. Natl. Acad. Sci. U. S. A. **100:**15655–15660.
24. **Parks, R. J., and D. H. Evans.** 1991. Effect of marker distance and orientation on recombinant formation in poxvirus-infected cells. J. Virol. **65:**1263–1272.
25. **Parrish, S., W. Resch, and B. Moss.** 2007. Vaccinia virus D10 protein has mRNA decapping activity, providing a mechanism for control of host and viral gene expression. Proc. Natl. Acad. Sci. U. S. A. **104:**2139–2144.
26. **Rice, A. P., and B. E. Roberts.** 1983. Vaccinia virus induces cellular mRNA degradation. J. Virol. **47:**529–539.
27. **Schramm, B., C. A. de Haan, J. Young, L. Doglio, S. Schleich, C. Reese, A. V. Popov, W. Steffen, T. Schroer, and J. K. Locker.** 2006. Vaccinia-virus-induced cellular contractility facilitates the subcellular localization of the viral replication sites. Traffic **7:**1352–1367.
28. **Seto, J., L. M. Celenza, R. C. Condit, and E. G. Niles.** 1987. Genetic map of the vaccinia virus HindIII D fragment. Virology **160:**110–119.
29. **Stahl, F. W.** 1979. Genetic recombination: thinking about it in phage and fungi. W. H. Freeman, San Francisco, CA.
30. **Tolonen, N., L. Doglio, S. Schleich, and J. Krijnse Locker.** 2001. Vaccinia virus DNA replication occurs in endoplasmic reticulum-enclosed cytoplasmic mini-nuclei. Mol. Biol. Cell **12:**2031–2046.
31. **Weir, J. P., G. Bajszar, and B. Moss.** 1982. Mapping of the vaccinia virus thymidine kinase gene by marker rescue and by cell-free translation of selected mRNA. Proc. Natl. Acad. Sci. U. S. A. **79:**1210–1214.
32. **Wiebe, M. S., and P. Traktman.** 2007. Poxviral B1 kinase overcomes barrier to autointegration factor, a host defense against virus replication. Cell Host Microbe **1:**187–197.
33. **Willer, D. O., M. J. Mann, W. Zhang, and D. H. Evans.** 1999. Vaccinia virus DNA polymerase promotes DNA pairing and strand-transfer reactions. Virology **257:**511–523.
34. **Yao, X. D., and D. H. Evans.** 2003. Characterization of the recombinant joints formed by single-strand annealing reactions in vaccinia virus-infected cells. Virology **308:**147–156.